Extremely Durable, Flexible Supercapacitors with Greatly Improved Performance at High Temperatures

Sung-Kon Kim,[†] Hae Jin Kim,[‡] Jong-Chan Lee,[§] Paul V. Braun,[†] and Ho Seok Park*,[⊥]

[†]Department of Materials Science and Engineering, Frederick Seitz Materials Research Laboratory, Beckman Institute for Advanced Science and Technology, University of Illinois at Urbana—Champaign, Urbana, Illinois 61801, United States, [‡]Division of Material Science, Korea Basic Science Institute, 113 Gwahangno, Yuseong-gu, Daejeon 305-333, Republic of Korea, [§]Department of Chemical and Biological Engineering and Institute of Chemical Process, Seoul National University, 599 Gwanak-ro, Gwanak-gu, Seoul 151-744, Republic of Korea, and [⊥]School of Chemical Engineering, Sungkyunkwan University (SKKU), Suwon 440-746, Republic of Korea

ABSTRACT The reliability and durability of energy storage devices are as important as their essential characteristics (*e.g.*, energy and power density) for stable power output and long lifespan and thus much more crucial under harsh conditions. However, energy storage under extreme conditions is still a big challenge because of unavoidable performance decays and the inevitable damage of components. Here, we report high-temperature operating, flexible supercapacitors (f-SCs) that can provide reliable power output and extreme durability under severe electrochemical, mechanical, and thermal conditions. The outstanding capacitive features (*e.g.*, ~40% enhancement of the rate capability and a maximum capacitances of 170 F g^{-1} and 18.7 mF cm^{-2} at 160 °C) are attributed to facilitated ion transport at elevated temperatures. Under high-temperature operation and/or a flexibility test in both static and dynamic modes at elevated temperatures >100 °C, the f-SCs showed extreme long-term stability of 100000 cycles (>93% of initial capacitance value) and mechanical durability after hundreds of bending cycles (at bend angles of 60—180°). Even at 120 °C, the versatile design of tandem serial and parallel f-SCs was demonstrated to provide both desirable energy and power requirements at high temperatures.

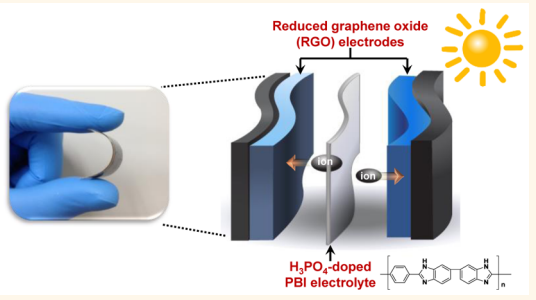

KEYWORDS: energy storage · supercapacitor · high temperature · polybenzimidazole · graphene

Temperature is an important variable that can determine the performance, life-span, and safety in energy storage.[1,2] Given that electrochemical reactions and transport phenomena are coupled and promoted at elevated temperatures, following Arrhenius' law,[3] at high temperatures, energy-storage devices deliver more power and exhibit greater capacity due to faster reaction kinetics and charge carrier mobility.[4,5] Operating energy storage devices at high temperatures >100 °C is essential for harsh demanding applications such as automotive, aerospace, solar/wind energy, and ultrahigh power electronics.[6,7] However, it remains challenging:[4] performance degradation is caused by the loss of active material and increased internal resistance,[8−10] thermal runaway is triggered by thermochemical and electrical heating,[4] and safety issues are present in the undesirable side reactions and the volatility and flammability of liquid electrolytes.[4] Particularly problematic in real-world applications are the thermal stresses of energy storage devices under external circumstances (*e.g.*, heat from the surroundings such as electronic circuit, vehicle engines, desert, and hot climates) that can cause permanent damage or complete failure of the cell.[11] Existing energy storage devices cannot avoid the aforementioned issues, resulting in their own shortcomings: lithium ion and sodium batteries, whose respective operating temperatures of about 70 °C[3,12] and >300 °C are out of range for practical applications, have low power, short cycle life, and a lack of safety. Additionally, conventional capacitors show very limited energy density and poor thermal stability. Breakthroughs are needed to enable highly durable and reliable energy storage devices that can be well operated under severe electrochemical, mechanical, and thermal conditions, possibly leading to

* Address correspondence to phs0727@skku.edu.

Received for review June 19, 2015 and accepted July 20, 2015.

Published online July 20, 2015
10.1021/acsnano.5b03732

satisfactory performance comparable to or greater than that typically available for near-room-temperature operation.

With the ever-increasing demand for energy storage under extreme conditions, flexible solid-state energy storage devices have been extensively investigated for next-generation electronic and biomedical applications. High-performance flexible supercapacitors (f-SCs) are attractive for a number of these applications because they can provide higher power, faster charge/discharge rates, greater cycle life, and safer operation than secondary batteries.[13−18] However, the performance of existing SCs at temperatures >100 °C is still unsatisfactory due to the rapid increase in internal resistance with temperature by loss of proton media and insufficient thermal stability of the device components.[19,20] Thermal and design issues of energy storage devices are strongly demanding for space-limited applications where cooling is difficult or impossible. For example, the machinery space of hybrid electric vehicle, aerospace, and military systems is restricted in volume and mass and can be subjected to operating temperatures of at least 120 °C. Flexibility enables versatile design, which is needed to make better use of the given space for compact integration.[21] Ajayan *et al.* recently demonstrated a SC operating up to 200 °C using clay−ionic liquid composite electrolyte,[22] but neither flexibility nor durability has been explored. Establishment of a fundamental foundation of ion dynamics at high temperatures in SCs would enable performance enhancements necessary to supply a stable and reliable power source under harsh conditions.[5,11,22−27]

Herein, we developed a flexible and durable SC consisting of a phosphoric acid (H_3PO_4)-doped poly[2,2′-*m*-phenylene-5,5′-bibenzimidazole] (PBI) electrolyte sandwiched between two pristine reduced graphene oxide (RGO) flexible films as shown in Figure 1. The integrated SC showed good capacitive behaviors under extreme conditions such as thermal, mechanical, and electrochemical stresses and holds great promise for use in f-SCs under harsh conditions.

RESULTS AND DISCUSSION

Of the current state-of-the-art polymer electrolytes that are the most important circuit component in determining the high-temperature performance of SCs,[13−16] H_3PO_4-doped PBIs (with thickness of ∼50 μm) were chosen for their superior performance and mechanical integrity at elevated temperatures.[28] Along with the nonvolatile nature of H_3PO_4 and the prominent thermal stability of PBI (see Figure S1), the H_3PO_4-doped PBI electrolytes display a high ionic conductivity of ∼0.1 S cm^{-1} at temperatures >100 °C under low relative humidity <50% while maintaining their mechanical robustness and flexibility (see Figure S2). RGO films were used as a bifunctional material of the active

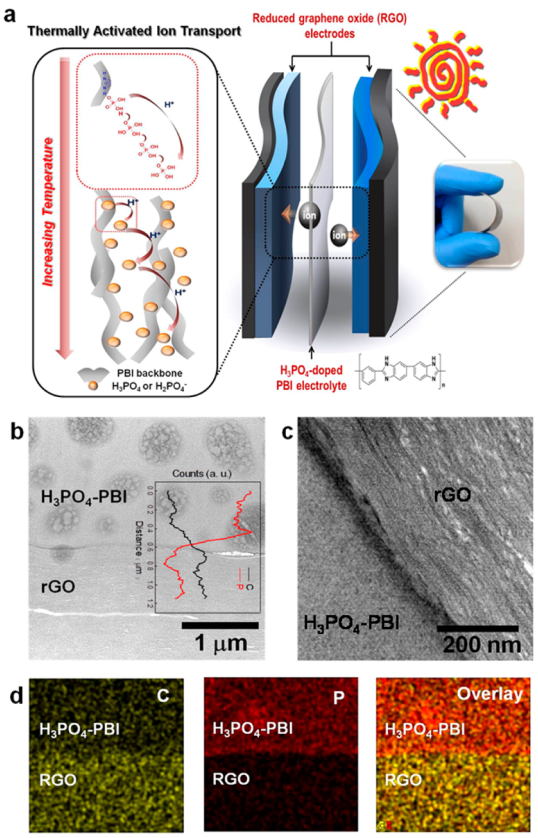

Figure 1. (a) Schematic view and photograph of a high-temperature operating, flexible RGO-PBI SC (right) and thermally activated, nanoscale-confined ionic transport at elevated temperatures (left). (b) SEM cross-sectional image of RGO-PBI SC milled by FIB. Inset is line EDS profiles of carbon and phosphorus. (c) TEM cross-sectional image of RGO-PBI SC milled by FIB. (d) EDS elementary mapping images of carbon, phosphorus, and overlay corresponding to SEM image of (b). (b−d) All images were taken after 100000 GCD cycles at 1.8 A g^{-1} and 120 °C.

electrode and the current collector for the simplified configuration owing to their high electrical conductivity, thermal stability, and mechanical integrity.[29−31] The solution-processable RGOs can be easily assembled into a flexible and resilient thin film without a thermolabile insulating binder or conducting agent of low capacitance. These would induce important features of lower equivalent series resistance (ESR), better thermal stability, and greater specific capacitances than additive-containing electrodes.[32,33] In this study, ∼1 μm thick, internetworked, and compact RGO films prepared by directional convective assembly were determined to be optimal (see the Supporting Information and Figure S3).[34] Solid-state RGO-PBI f-SCs were successfully integrated through simple fabrication procedures (Figure 1a and see the Experimental Section in the Supporting Information). The electrochemical properties of all devices fabricated were characterized under various conditions using a home-made instrument (see Figure S4 and movie S1).

To evaluate the feasibility of RGO-PBI SCs as high-temperature operating, flexible energy storage devices,

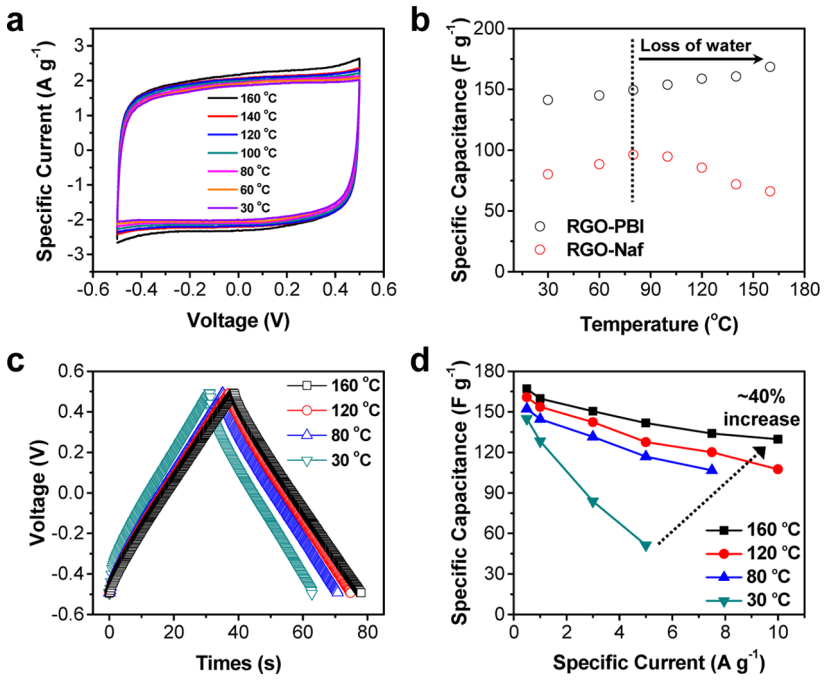

Figure 2. (a) CV curves of RGO-PBI SC measured at a scan rate of 50 mV s^{-1} in the temperature range of 30−160 °C. (b) Plots of temperature *vs* specific capacitance of RGO-PBI and RGO-Naf SCs calculated from the CV curves at a scan rate of 50 mV s^{-1}. (c) GCD curves of RGO-PBI SC in the temperature range of 30−160 °C measured at a specific current of 1 A g^{-1}. (d) Rate capability of RGO-PBI SC in the temperature range of 30−160 °C measured at different specific currents.

we investigated their electrochemical behavior using cyclic voltammetry (CV) and galvanostatic charge/discharge (GCD) tests as shown in Figure 2. The CV and GCD curves were practically measured in a two-electrode configuration after a steady state at each temperature ranging from 30 to 160 °C. RGO-Nafion (Naf) SCs were used as a control sample (see Figure S5) because they are well-understood and Nafion117 is a representative electrolyte for solid-state electrochemical devices.[35] The specific capacitances (80 F g^{-1} at 50 mV s^{-1}) of RGO-Naf SCs at room temperature are consistent with those previously reported (Figure 2b).[34,35] As the temperature increases, the specific capacitances of RGO-Naf SCs reach a maximum of 96 F g^{-1} at 80 °C and then dramatically decrease. Moreover, the CV curves of the RGO-Naf SCs change from a rectangular to a distorted shape at 80 °C due to an increase in ionic resistance, which is typically observed in other solid-state SCs due to loss of water.[11] In contrast, both rectangular CV and symmetric GCD profiles of the RGO-PBI SCs imply a near-ideal electrochemical double-layer capacitor (EDLC)-type behavior (Figure 2a,c). A low internal resistance, required for high power applications,[36] was verified by an immediate reversible change in current upon alternating the potential sweep of CV and a small IR drop of GCD.[19,37] Such a reversible capacitive behavior of the devices is preserved, even at 160 °C, indicating fast charge/discharge characteristics under thermal stresses. Notably, the RGO-PBI SCs show a gradual increase in stored charge with increasing temperature, achieving a maximum capacitance of ~170 F g^{-1} at 160 °C. In the GCD profiles, the specific capacitance value of the RGO-PBI SCs at 160 °C is ~25% greater than the value at 30 °C (Figure 2b). The areal and volumetric stack capacitances of RGO-PBI SCs are 18.7 mF cm^{-2} and 0.634 F cm^{-3} at 160 °C, respectively, comparable to or greater than other solid-state SCs measured at room temperature (see Figure S6).[36−40]

To investigate the temperature-dependent rate capability of RGO-PBI SCs, GCD curves were collected at specific currents from 0.5 to 10 A g^{-1} at varying temperatures (Figure 2c,d and see Figure S7). At 30 °C, large capacitance fading, a deviation from ideal capacitor behavior, and the larger IR drop are observed as the specific current increases by a factor of 10. As a result of the sluggish ion transport, the capacitance retention from 0.5 to 5 A g^{-1} is drastically dropped to 35%. As the temperature increases from 30 to 160 °C, the capacitance retention increases by 78% due to thermally activated ion transport. Both the highest capacitance of ~160 F g^{-1} and the ~40% enhancement in rate capability at 160 °C are the first recorded measurements for high temperature f-SCs.

For a comprehensive understanding of the unique capacitive behavior of RGO-PBI SCs, the nanoscale confined ion transport at elevated temperatures was analyzed as shown in Figure 3. The capacitive behaviors of f-SCs at a macroscopic level are governed by the ion transport activated at elevated temperatures. The activation energy of the SCs derived from the Arrhenius equation is found to be 8.49 kJ mol^{-1}, which

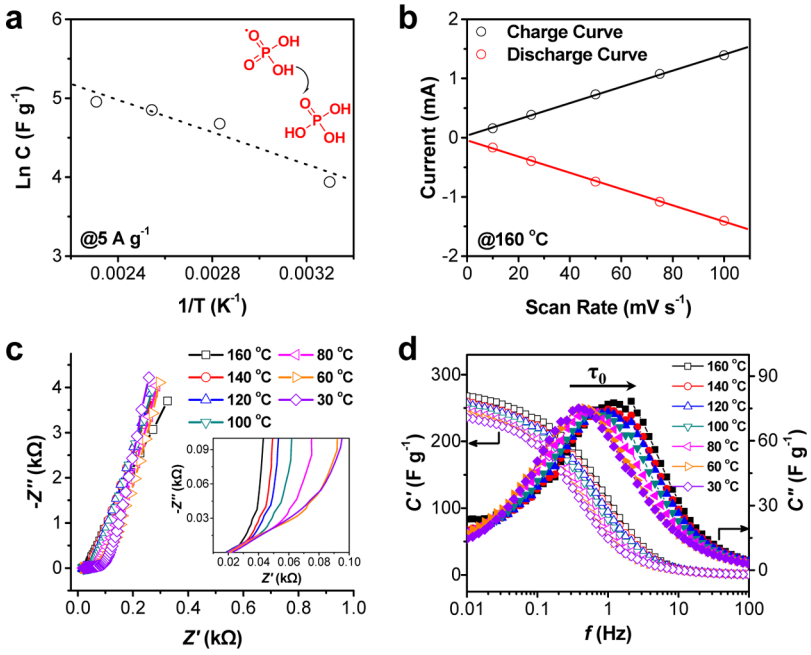

Figure 3. (a) Arrhenius plot of specific capacitance *vs* inverse temperature for the kinetics of ionic transport. (b) Plots of scan rate (10 to 100 mV s^{-1}) *vs* capacitive current (extracted from the CV curves at 0 V) measured at 160 °C for the charge (R^2 = 0.9993) and discharge (R^2 = 0.9994) curves. (c) Nyquist plots of RGO-PBI SC in the temperature range of 30 to 160 °C. (Inset) Magnified plots in the high-frequency region. (d) Plots of frequency *vs* real (*C*′) and imaginary (*C*″) part capacitances of RGO-PBI SC in the temperature range of 30−160 °C.

is comparable to the energy barrier for the ion transport of PBI-H_3PO_4 system through an ion-hopping mechanism, or the Grotthuss mechanism (Figure 3a and see Figure S2).[31,41] The electrochemical behavior at temperatures >100 °C is converged to a surface-controlled system, corresponding to a linear relationship between the capacitive current and the scan rate, which is crucial for high power applications under extreme conditions (Figure 3b and see Figure S8).[30] Moreover, the frequency response of the f-SCs, which was analyzed by electrochemical impedance spectroscopy (EIS), provides the information on device dynamics (Figure 3c,d). No evident semicircle is observed in the Nyquist plot, indicating low interfacial resistance due to good device integration as proven by SEM image (Figures 1b). As the temperature increases from 30 to 160 °C, the charge-transfer resistances of the SCs decrease from 3.4 to 0.5 Ω, and the ESRs of the SCs, that were observed at the intercept of the real axis (Z′) of the Nyquist plot, are also reduced from 23 to 18 Ω and a more vertical line is observed in the low frequency ranges, close to an ideal capacitive behavior.[42] To better understand the kinetics as a function of operating temperature, the relaxation time constant (τ_0) was derived from the imaginary part of the complex capacitance $C''(\omega)$ corresponding to the dielectric loss of the electrolyte (Figure 3d).[42] As the temperature increases, the peak maximum frequency shifts to a higher value and the τ_0 values decrease from 2.61 s at 30 °C to 0.826 s at 160 °C. Since the τ_0 is correlated with the characteristic time required for full discharge, it is shortened here because of the fast ion transport, and not because of the electronic conduction.[43] The fast ion mobility of the free carriers can be conferred as the kinetics is promoted by overcoming the activation energy barrier at high temperatures through the structural diffusion of ionic defects modulated by hydrogen-bond-breaking and -forming processes (Figure 1a and see the Supporting Information).[5,44] Accordingly, the ion transport into the storage sites of the electrode surface is a key to achieving good capacitive and rate performances at high temperatures. Despite using the same electrodes as the thin RGO films of RGO-PBI SCs, a control RGO-Naf SC shows dramatic performance degradation at high temperatures due to the decrease in ionic conductivity arising from the loss of water, which acts as a transporting medium in the hydrated polymer electrolyte. Accordingly, high-performance solid-state SCs at temperatures >100 °C are not feasible with a conventional polymer electrolyte as a consequence of the drastic increase in ionic resistance below the critical humidity. By contrast, when PBI electrolytes were doped with nonvolatile H_3PO_4, the ionic transport (ionic conductivity of ∼0.1 S cm^{-1}) is facilitated through an ion-hopping mechanism as the temperature increased above 100 °C at a low humidity of less than 50%.[28] Therefore, the capacitive and rate performances of the RGO-PBI SCs at high temperatures were greatly improved by the facilitated ion transport kinetics at the electrode/electrolyte interface.

Excellent durability of the RGO-PBI SCs was demonstrated, even under electrochemical, thermal, and

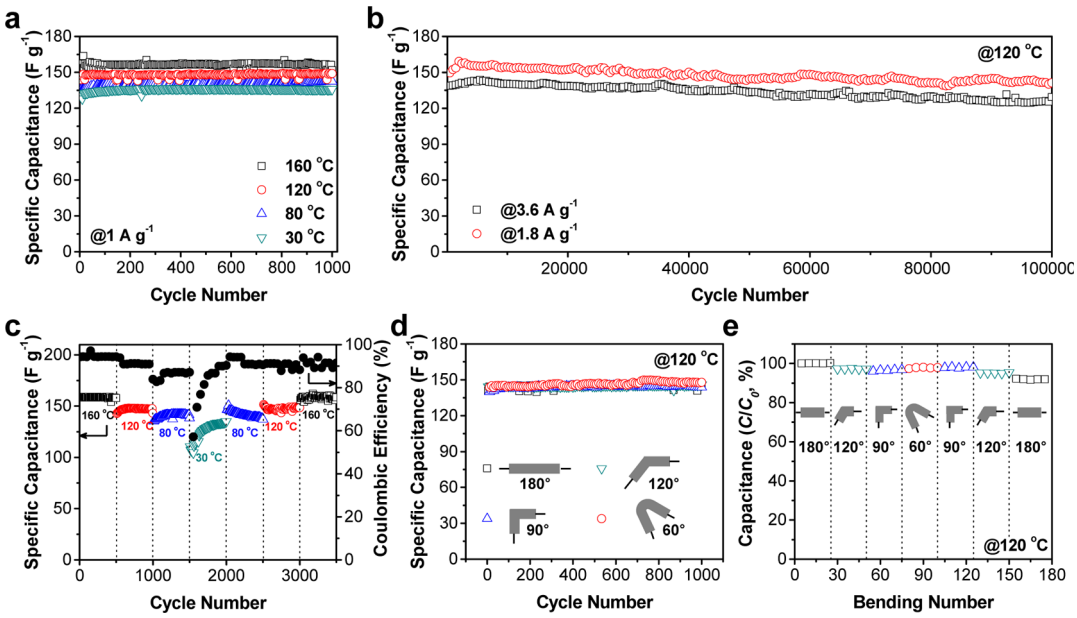

Figure 4. (a) Cyclic stability (1000 GCD cycles at 1 A g^{-1}) of RGO-PBI SC in the temperature range of 30−160 °C. (b) Ultra-long-term stability (100000 GCD cycles at 1.8 and 3.6 A g^{-1}) of RGO-PBI SC measured at 120 °C. (c) Long-term stability (3500 GCD cycles at 1 A g^{-1}) of RGO-PBI SC under dynamic thermal stresses (temperature variations per 500 cycles). (d) Cyclic stability (1000 GCD cycles at 1 A g^{-1}) of RGO-PBI SC measured at 120 °C under mechanical stresses (bend angles of 60°, 90°, and 120° with radii of curvature of 17, 7.2, and 5.7 mm, respectively). (e) Normalized specific capacitance (C/C_0 (%) where C_0 and C correspond to the capacitances before and after cycles, respectively) of RGO-PBI SC under different bend angles (60° to 180°) and bending number (up to 180) at 120 °C and 1 A g^{-1}.

mechanical stresses, in Figure 4. As shown in the GCD curves at 1 A g^{-1} (Figure 4a), the SCs preserve their initial capacitances for at least 1000 cycles over a temperature range of 30 to 160 °C. After 100000 charge/discharge cycles at 120 °C, importantly, the capacitances of the SCs at 1.8 and 3.6 A g^{-1} are conserved by ~93%, which is first demonstrated in solid-state energy storage devices (Figure 4b). Lifetime tests of SCs under more severe conditions (temperature cycling) were conducted (Figure 4c). In over 3500 charge/discharge cycles during thermal cycling there are no notable attenuations of the capacitances, and high Coulombic efficiencies are observed; the specific capacitances measured at each temperature remain constant with marginal fluctuations. For example, the specific capacitance at 160 °C prior to cooling is 158 F g^{-1}, and after reheating to 160 °C, the initial value is recovered in full. The feasibility of SCs as high-performance, flexible-energy storage devices at high temperatures was confirmed by performing flexibility tests under bend angles of 60°, 90°, and 120° (13, 7.2, and 5.8 mm of bend radii, respectively, Figure 4d). Even in the various bent states at 120 °C, the SCs achieve ~100% capacitance retention after 1000 cycles. In a dynamic modes of flexibility test (180 straight-bending-straight cycles at 120 °C), the capacitance degradation is below 9% of the initial value (Figure 4e). These results highlight that RGO-PBI SCs can deliver stable power output and reliable operation under harsh conditions, including ultralong cycles, temperature circulation, and mechanical stresses.

We next discuss why the RGO-PBI SCs can achieve the exceptional durability in terms of the following aspects: (1) The key device components such as electrode and electrolyte are thermally, mechanically, and electrochemically stable. As demonstrated in the cross-sectional SEM and TEM images prepared by a focused-ion beam (FIB) microscope before and after long-term operation in extreme conditions (Figure 1b,c and see Figure S9), no distinct deformation in the bulk and interface structure is observed because of the good adhesion at the electrolyte/electrode interface and their intrinsic durability. This device consolidation results in improved cyclic performance, even under severe bending and thermal tests.[34] (2) The ion carriers in the RGO interlayers, as shown in energy dispersive spectrometry (EDS) elementary mapping images (Figure 1d), are remarkably stable, resulting from the thermal and electrochemical durability of nanoscale confined H_3PO_4 acting as hopping sites. Such a nanoscale confinement is triggered by the penetration of the H_3PO_4 electrolyte that was squeezed out of the H_3PO_4-doped PBI in the course of hot pressing. The interstitial diffusion of the H_3PO_4 electrolytes into the interlayers of RGO sheets during device integration is evinced by the observable increase in the thickness of the RGO film and by the chemical identity and thickness-dependent distribution of the H_3PO_4 electrolyte inside the RGO electrodes as confirmed by a phosphorus signal of EDS profiles (see Figures S9b and S9d). Even after 100000 cycles at 120 °C, the nanoscale confined ions are observed by the existence of phosphorus

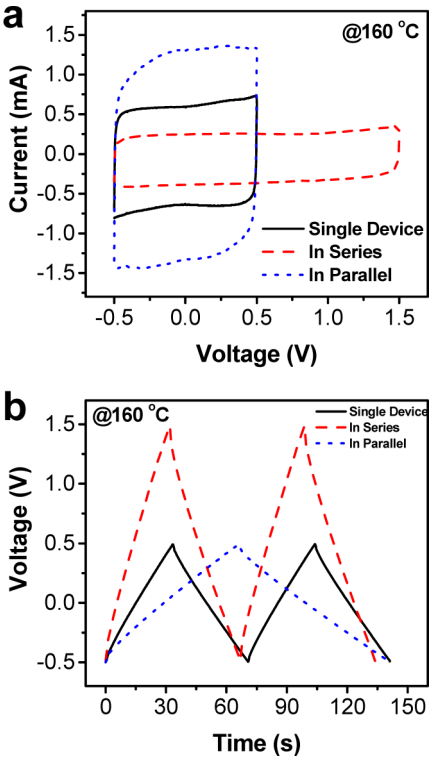

Figure 5. (a) CV curves at a scan rate of 50 mV s^{-1} and (b) GCD curves at a constant current of 0.4 mA for the single and tandem RGO-PBI SCs assembled in series and parallel at 160 °C.

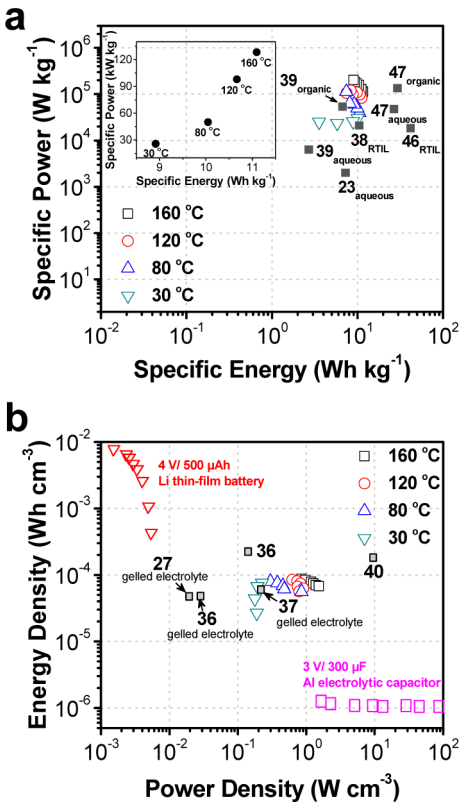

Figure 6. (a) Gravimetric (per kilogram of electrode) and (b) volumetric (per cm^3 of stack) energy and power density of RGO-PBI SC measured in the temperature range of 30−160 °C with values previously reported in the literatures (numbers and subscripts in figures denote references and electrolytes used, respectively). The data for the Li thin-film battery and Al electrolytic capacitor are referred from refs 37 and 40.

in the EDS mappings (Figure 1d). Furthermore, the confinement of ions can prevent restacking of isolated RGO layers for easy access of ions to the adsorption sites at high temperatures,[45] leading to prewetting of the electrode surfaces for the reduced ion resistance.

To provide both desirable energy and power requirements at high temperatures, we constructed tandem SCs, where single cells were connected in series and in parallel as shown in Figure 5. Series and parallel tandem SCs offer significant advantages, including an extension of the operating voltage window and an increase in the capacitive currents, respectively.[15,37] CV and GCD curves of the series and parallel tandem RGO-PBI SCs were measured at 160 °C. The tandem serial SC provides a broader, reversible operating voltage window up to ~2.0 *vs* ~1.0 V for a single SC. Tandem parallel SCs increase the output current by a factor of 2 over a single SC while maintaining a reversible capacitive behavior within a 1.0 V window. Even at 120 °C, a device of three RGO-PBI SCs linked in series can light a red light-emitting-diode (LED) with the lowest working potential of 2.0 V (see Figure S10 and movie S2). Thus, the versatile design prospects of tandem SCs, as well as their durability, yield large energy, and power densities at elevated temperatures.

The specific and volumetric power (*P*) and energy (*E*) of the RGO-PBI SCs are evaluated as a function of temperature as shown in Figure 6. As shown in the Ragone plot, the specific *P* and *E* improved with increasing temperature (Figure 6a). RGO-PBI SCs can provide a maximum specific *P* of ~203 kW kg^{-1} (with a specific *E* of 9 Wh kg^{-1}) and a maximum specific *E* of ~11 Wh kg^{-1} (with a specific *P* of 113 kW kg^{-1}) at 160 °C. These values (based on electrodes mass) are greater than those of state-of-the-art solid-state SCs and are even close to those of solid-state pseudocapacitors.[23,38,39,46,47] Volumetric *E* and *P* density (per cm^3 of stack) of the RGO-PBI SCs are ~0.08 mWh cm^{-3} (100 times higher than that of the Al electrolytic capacitor) and ~1.5 W cm^{-3} (300 times higher than that of the 500 μAh lithium thin film battery), respectively, which are comparable to or even higher than those of solid-state SCs based on carbon nanomaterials (Figure 6b).[27,36,37]

CONCLUSION

We have demonstrated extremely durable f-SCs prepared by integrating bifunctional H_3PO_4-doped PBI electrolytes and RGO films. Despite the simple configuration, the resultant devices are sufficiently adaptable under electrochemical, thermal, and mechanical

stresses to preserve their performance, with great improvement in the most severe conditions. A new generation of f-SCs, with the long-term durability and outstanding electrochemical properties, were realized, showing a high position of the Ragone plot, even under severe conditions. This study provides a fundamental understanding of the unusual electrochemical behavior of solid-state SCs in the ion-transport dominating regime and rational design guidelines for various electrochemical devices such as fuel cells, solar cells, actuators, sensors, batteries, and supercapacitors that are operated under harsh circumstances.

EXPERIMENTAL SECTION

Fabrication of RGO-PBI and RGO-Naf SCs. PBI was synthesized as previously reported (see the Supporting Information for details).[48] Graphene oxides (GOs) were synthesized from graphite powder (powder, <20 μM, Aldrich) using the modified Hummer method.[34,49] The sequence of experimental steps applied during the preparation of RGO starting from GO is as follows. First, 5 mg of as-prepared GOs was fully exfoliated in 10 mL of deionized (DI) water (ca. 0.5 mg mL^{-1}). GOs dispersed in DI water were reduced with a 100 μL hydrazine solution (35 wt % in water, Aldrich) at 90 °C for 4 h to produce a homogeneous black dispersion that was then filtered through an anodic alumina oxide (AAO) membrane filter (47 mm diameter, 0.2 μm pore size, Whatman) under vacuum. Once the filtration was completed, the resulting RGO films were purified in DI water several times to remove the residual ammonia and hydrazine and then dried in a ventilated oven at 80 °C for 12 h. To obtain a freestanding film, the thin RGO films were carefully peeled off the membrane filter and cut into required sizes for various electrode tests. All solid-state f-SCs were assembled in a two-electrode configuration with symmetrical RGO film electrodes. The H_3PO_4-doped PBI membrane as both the electrolyte and separator was sandwiched between two thin RGO films that served as both electrodes and was transferred to the poly(ethylene terephthalate) (PET) substrates, where thin gold films as a current collector were deposited on the edge of each RGO film by the electron-beam evaporation technique. Hot pressing at 3 tons and 130 °C for 3 min was applied to improve contact between the electrolyte and electrodes. The resultant SC was annealed at 90 °C for 12 h prior to use. Two-sided, flexible silicon rubber heating pads were used to thoroughly enclose the as-prepared SC for analytical measurements at high temperatures.

RGO-Nafion117 (Naf) SC used as a control sample was prepared by assembly of a Nafion117 (N117) film acting as both the electrolyte and separator sandwiched between the two RGO thin film electrodes. The geometry of RGO-Naf SCs was identical to that of RGO-PBI SCs. The N117 membrane was purchased from Aldrich and treated with a hot 5 wt % H_2O_2 aqueous solution for 1 h and boiling 1 M H_2SO_4 aqueous solution for 1 h. The membrane was washed several times with deionized water and then dried using a gel dryer at 60 °C for 1 h. The procedure for preparation of RGO-Naf SC is in line with that for the preparation of RGO-PBI SC, except for the dipping and drying conditions. After the assembling and hot pressing steps of the RGO/N117/RGO, the SC was immersed in a 1 M H_2SO_4 solution and dried at 60 °C for 12 h prior to use.

Characterization. Thermal gravimetric analysis (TGA, PerkinElmer Inc., USA) was carried out in air at temperatures ranging from 30 to 800 °C at a heating rate of 10 °C min^{-1}. The morphological properties were probed by a focused-ion beam/scanning electron microscope (FIB/SEM) instrument (Quanta 3D FEG, FEI). The platinum layer deposition protected the near-surface features because the depth of damage was significantly reduced. To mill a cross-section with the FIB, gallium ion (Ga^+) was accelerated with an energy of 30 keV toward the sample. Cross sections were milled perpendicular to the surface with a 10 μm depth. TEM images were collected on a JEM-2100F (200 kV, JEOL). The electrochemical characteristics were evaluated by cyclic voltammetry (CV) using a CHI 760D electrochemical workstation (CH Instruments) and galvanostatic charge/discharge (GCD) using an Iviumstat.XR (Ivium Technologies). CV measurements were performed at different scan rates from 10 to 100 mV s^{-1}. GCD measurements were performed at different specific currents of 0.5 to 10 A g^{-1}. In the GCD profiles, the specific capacitance of the two-electrode configuration can be estimated using the following equation[25]

$$C = 2I/[(\Delta V/\Delta t)m] \quad (1)$$

where I is the current applied, $\Delta V/\Delta t$ is the slope of the discharge curve after IR drop at the beginning of the discharge curve, and m is the average mass of two RGO electrodes. Activation energy was computed according to the following formula[31]

$$C = C_0 \exp(-Q/RT) \quad \text{or} \quad \ln C = \ln C_0 - Q/RT \quad (2)$$

where C is the amount of charge accumulated at the electrode/electrolyte interface enabled by the molecular or ionic motion mechanism, C_0 is a pre-exponential factor, Q is the activation energy, T is the absolute temperature, and R is the universal gas constant. To decouple the bulk and interface electrochemistry of the device, electrochemical impedance spectroscopy (EIS) was measured at the open-circuit voltage by applying an alternating potential with a 10 mV amplitude over a frequency range of 10^6–10^{-2} Hz using the CHI 760D. Equivalent series resistances (ESRs) of the SCs were obtained from the intercept of the curve on the x-axis. The relaxation time corresponding to the dielectric loss of the electrolyte was obtained from the frequency (f_0) at the maximal $C''(\omega)$ following the equation of $\tau_0 = 1/f_0$. The SC life cycling tests were performed by measuring GCD cycles with varying temperature ranges (30–160 °C) and mechanical stresses (13, 7.2, and 5.8 mm of bend radii) at a constant specific current. Temperature-changing tests were conducted by altering the temperature (160 °C → 120 °C → 80 °C → 30 °C → 80 °C → 120 °C → 160 °C) per 500 cycles up to 3500 cycles at a constant specific current of 1 A g^{-1}. The mechanical stability of SC was confirmed by estimating GCD curves before and after 180 straight-bending-straight-bending cycles with bend angles of 60° to 180° at 120 °C and 1 A g^{-1}. An ultralong SC life was proved by measuring the GCD up to 100000 cycles at 120 °C and a constant specific current of 3.6 and 1.8 A g^{-1}. The specific power (P) and energy (E) were calculated using the following equation[47]

$$P = (\Delta V)^2/4RM, \quad E = 0.5C(\Delta V)^2/M \quad (3)$$

where ΔV, R, and C are the potential window of discharge, internal resistance from IR drop, and total mass of both electrodes, respectively. The internal resistance was computed from the voltage drop at the beginning of each discharge

$$R = \Delta V_{iR}/2i \quad (4)$$

where ΔV_{iR} and i are the voltage drop between the first two points in the voltage drop at the top cutoff and applied current, respectively. The volumetric P and E density were based on volume (cm^3) of stack that includes two RGO films, H_3PO_4-doped PBI electrolyte, and two gold-coated PET substrates.

Conflict of Interest: The authors declare no competing financial interest.

Supporting Information Available: Additional information on experimental methods, optimization of SC thickness, ion-transport mechanism, TGA, ionic conductivity, SEM, CV, GCD, areal and stack capacitances, and EDS and movies (SC operation and light a red LED). The Supporting Information is available free of charge on the ACS Publications website at DOI: 10.1021/acsnano.5b03732.

Acknowledgment. We acknowledge financial support by the National Research Foundation of Korea Grant funded by the Korean Government (NRF-2010-C1AAA001-0029018 and NRF-2013-220-2013S1A2A2035510). We thank Dr. Yury Gogotsi at Drexel University for valuable comments on the interpretation of SC performance and Dr. Jin-Gyu Kim at Korea Basic Science Institute (KBSI) for helpful discussions and assistance in FIB sample preparation and characterization. H.S.P. conceived and led the project. S.-K.K. performed experiments of materials synthesis and device fabrication. H.S.P. and S.-K.K. analyzed the data. All authors discussed the results and co-wrote the manuscript.

REFERENCES AND NOTES

1. Béguin, F.; Frąckowiak, E. *Supercapacitors: Materials, Systems, and Applications*; Wiley−VCH: Weinheim, 2013.
2. Conway, B. E. *Electrochemical Supercapacitors: Scientific Fundamentals and Technological Applications*; Kluwer Academic/Plenum: New York, 1999.
3. Xu, K. Nonaqueous Liquid Electrolytes for Lithium-Based Rechargeable Batteries. *Chem. Rev.* **2004**, *104*, 4303–4418.
4. Bandhauer, T. M.; Garimella, S.; Fuller, T. F. A Critical Review of Thermal Issues in Lithium-Ion Batteries. *J. Electrochem. Soc.* **2011**, *158*, R1–R25.
5. Hung, K.; Masarapu, C.; Ko, T.; Wei, B. Wide-Temperature Range Operation Supercapacitors from Nanostructured Activated Carbon Fabric. *J. Power Sources* **2009**, *193*, 944–949.
6. Xiong, G.; Kundu, A.; Fisher, T. S. *Thermal Effects in Supercapacitors*; Springer: New York, 2015.
7. Hastak, R. S.; Sivaraman, P.; Potphode, D. D.; Shashidhara, K.; Samui, A. B. All solid supercapacitor based on activated carbon and poly[2,5-benzimidazole] for high temperature application. *Electrochim. Acta* **2012**, *59*, 296–303.
8. Hunter, J. C. Preparation of a New Crystal Form of Manganese Dioxide: λ-MnO_2. *J. Solid State Chem.* **1981**, *39*, 142–147.
9. Gummow, R. J.; de Kock, A.; Thackeray, M. M. Improved Capacity Retention in Rechargeable 4 V Lithium/Lithium-Manganese Oxide (Spinel) Cells. *Solid State Ionics* **1994**, *69*, 59–67.
10. Nakajima, H.; Ohno, H. Preparation of Thermally Stable Polymer Electrolytes from Imidazolium-Type Ionic Liquid Derivatives. *Polymer* **2005**, *46*, 11499–11504.
11. Lin, R.; Taberna, P.-L.; Fantini, S.; Presser, V.; Pérez, C. R.; Malbosc, F.; Rupesinghe, N. L.; Teo, K. B. K.; Gogotsi, Y.; Simon, P. Capacitive Energy Storage from −50 to 100 °C Using an Ionic Liquid Electrolyte. *J. Phys. Chem. Lett.* **2011**, *2*, 2396–2401.
12. Kötz, R.; Hahn, M.; Gallay, R. Temperature Behavior and Impedance Fundamentals of Supercapacitors. *J. Power Sources* **2006**, *154*, 550–555.
13. Gogotsi, Y.; Simon, P. True Performance Metrics in Electrochemical Energy Storage. *Science* **2011**, *334*, 917–918.
14. Simon, P.; Gogotsi, Y. Materials for Electrochemical Capacitors. *Nat. Mater.* **2008**, *7*, 845–854.
15. Miller, J. R.; Simon, P. Electrochemical Capacitors for Energy Management. *Science* **2008**, *321*, 651–652.
16. Chmiola, J.; Largeot, C.; Taberna, P.-L.; Simon, P.; Gogotsi, Y. Monolithic Carbide-Derived Carbon Films for Micro-Supercapacitors. *Science* **2010**, *328*, 480–483.
17. Xiong, G.; Meng, C.; Reifenberger, R. G.; Irazoqui, P. P.; Fisher, T. S. Graphitic Petal Electrodes for All-Solid-State Flexible Supercapacitors. *Adv. Energy Mater.* **2014**, *4*, 1300515.
18. Xiong, G.; Hembram, K. P. S. S.; Reifenberger, R. G.; Fisher, T. S. MnO_2-Coated Graphitic Petals for Supercapacitor Electrodes. *J. Power Sources* **2013**, *227*, 254–259.
19. Wee, G.; Larsson, O.; Srinivasan, M.; Berggren, M.; Crispin, X.; Mhaisalkar, S. Effect of the Ionic Conductivity on the Performance of Polyelectrolyte-Based Supercapacitors. *Adv. Funct. Mater.* **2010**, *20*, 4344–4350.
20. Armand, M.; Endres, F.; MacFarlane, D. R.; Ohno, H.; Scrosati, B. Ionic-Liquid Materials for the Electrochemical Challenges of the Future. *Nat. Mater.* **2009**, *8*, 621–629.
21. Zhou, G.; Li, F.; Cheng, H.-M. Progress in Flexible Lithium Batteries and Future Prospects. *Energy Environ. Sci.* **2014**, *7*, 1307–1338.
22. Borges, R. S.; Reddy, A. L. M.; Rodrigues, M.-T. F.; Gullapalli, H.; Balakrishnan, K.; Silva, G. G.; Ajayan, P. M. Supercapacitor Operating at 200 Degrees Celsius. *Sci. Rep.* **2013**, *3*, 2572.
23. Meng, C.; Liu, C.; Chen, L.; Hu, C.; Fan, S. Highly Flexible and All-Solid-State Paperlike Polymer Supercapacitors. *Nano Lett.* **2010**, *10*, 4025–4031.
24. Pushparaj, V. L.; Shaijumon, M. M.; Kumar, A.; Murugesan, S.; Ci, L.; Vajtai, R.; Linhardt, R. J.; Nalamasu, O.; Ajayan, P. M. Flexible Energy Storage Devices Based on Nanocomposite Paper. *Proc. Natl. Acad. Sci. U. S. A.* **2007**, *104*, 13574–13577.
25. Masarapu, C.; Zeng, H. F.; Hung, K. H.; Wei, B. Effect of Temperature on the Capacitance of Carbon Nanotube Supercapacitors. *ACS Nano* **2009**, *3*, 2199–2206.
26. Largeot, C.; Taberna, P. L.; Gogotsi, Y.; Simon, P. Microporous Carbon-Based Electrical Double Layer Capacitor Operating at High Temperature in Ionic Liquid Electrolyte. *Electrochem. Solid-State Lett.* **2011**, *14*, A174–A176.
27. Jung, H. Y.; Karimi, M. B.; Hahm, M. G.; Ajayan, P. M.; Jung, Y. J. Transparent, Flexible Supercapacitors from Nano-Engineered Carbon Films. *Sci. Rep.* **2012**, *2*, 773.
28. Li, Q.; Jensen, J. O.; Savinell, R. F.; Bjerrum, N. J. High Temperature Proton Exchange Membranes Based on Polybenzimidazoles for Fuel Cells. *Prog. Polym. Sci.* **2009**, *34*, 449–477.
29. Li, D.; Muller, M. B.; Gilje, S.; Kaner, R. B.; Wallace, G. G. Processable Aqueous Dispersions of Graphene Nanosheets. *Nat. Nanotechnol.* **2008**, *3*, 101–105.
30. Stoller, M. D.; Park, S.; Zhu, Y.; An, J.; Ruoff, R. S. Graphene-Based Ultracapacitors. *Nano Lett.* **2008**, *8*, 3498–3502.
31. Liu, C.; Yu, Z.; Neff, D.; Zhamu, A.; Jang, B. Z. Graphene-Based Supercapacitor with an Ultrahigh Energy Density. *Nano Lett.* **2010**, *10*, 4863–4868.
32. Talapatra, S.; Kar, S.; Pal, S. K.; Vajtai, R.; Ci, L.; Victor, P.; Shaijumon, M. M.; Kaur, S.; Nalamasu, O.; Ajayan, P. M. Direct Growth of Aligned Carbon Nanotubes on Bulk Metals. *Nat. Nanotechnol.* **2006**, *1*, 112–116.
33. Presser, V.; Heon, M.; Gogotsi, Y. Carbide-Derived Carbons − from Porous Networks to Nanotubes and Graphene. *Adv. Funct. Mater.* **2011**, *21*, 810–833.
34. Choi, B. G.; Hong, J.; Hong, W. H.; Hammond, P. T.; Park, H. S. Facilitated Ion Transport in All-Solid-State Flexible Supercapacitors. *ACS Nano* **2011**, *5*, 7205–7213.
35. Park, K.-W.; Ahn, H.-J.; Sung, Y.-E. All-Solid-State Supercapacitor Using a Nafion® Polymer Membrane and Its Hybridization with a Direct Methanol Fuel Cell. *J. Power Sources* **2002**, *109*, 500–506.
36. Yoo, J. J.; Balakrishnan, K.; Huang, J.; Meunier, V.; Sumpter, B. G.; Srivastava, A.; Conway, M.; Mohana Reddy, A. L.; Yu, J.; Vajtai, R.; Ajayan, P. M. Ultrathin Planar Graphene Supercapacitors. *Nano Lett.* **2011**, *11*, 1423–1427.
37. El-Kady, M. F.; Strong, V.; Dubin, S.; Kaner, R. B. Laser Scribing of High-Performance and Flexible Graphene-Based Electrochemical Capacitors. *Science* **2012**, *335*, 1326–1330.
38. Kang, Y. J.; Chun, S.-J.; Lee, S.-S.; Kim, B.-Y.; Kim, J. H.; Chung, H.; Lee, S.-Y.; Kim, W. All-Solid-State Flexible Supercapacitors Fabricated with Bacterial Nanocellulose Papers, Carbon Nanotubes, and Triblock-Copolymer Ion Gels. *ACS Nano* **2012**, *6*, 6400–6406.
39. Kaempgen, M.; Chan, C. K.; Ma, J.; Cui, Y.; Gruner, G. Printable Thin Film Supercapacitors Using Single-Walled Carbon Nanotubes. *Nano Lett.* **2009**, *9*, 1872–1876.
40. Gao, W.; Singh, N.; Song, L.; Liu, Z.; Reddy, A. L. M.; Ci, L.; Vajtai, R.; Zhang, Q.; Wei, B.; Ajayan, P. M. Direct Laser Writing of Micro-Supercapacitors on Hydrated Graphite Oxide Films. *Nat. Nanotechnol.* **2011**, *6*, 496–500.
41. Bureiko, S. F.; Denisov, G. S. Dynamics of Molecular Hydrogen Exchange in Hydrogen-Bonded Systems. *Pol. J. Chem.* **2002**, *76*, 1177–1190.
42. Taberna, P. L.; Simon, P.; Fauvarque, J. F. Electrochemical Characteristics and Impedance Spectroscopy Studies of

Carbon-Carbon Supercapacitors. *J. Electrochem. Soc.* **2003**, *150*, A292–A300.
43. Pech, D.; Brunet, M.; Durou, H.; Huang, P.; Mochalin, V.; Gogotsi, Y.; Taberna, P.-L.; Simon, P. Ultrahigh-Power Micrometre-Sized Supercapacitors Based on Onion-Like Carbon. *Nat. Nanotechnol.* **2010**, *5*, 651–654.
44. Jiménez-García, L.; Kaltbeitzel, A.; Enkelmann, V.; Gutmann, J. S.; Klapper, M.; Müllen, K. Organic Proton-Conducting Molecules as Solid-State Separator Materials for Fuel Cell Applications. *Adv. Funct. Mater.* **2011**, *21*, 2216–2224.
45. Yang, X.; Zhu, J.; Qiu, L.; Li, D. Bioinspired Effective Prevention of Restacking in Multilayered Graphene Films: Towards the Next Generation of High-Performance Supercapacitors. *Adv. Mater.* **2011**, *23*, 2833–2838.
46. Kim, T. Y.; Lee, H. W.; Stoller, M.; Dreyer, D. R.; Bielawski, C. W.; Ruoff, R. S.; Suh, K. S. High-Performance Supercapacitors Based on Poly(ionic liquid)-Modified Graphene Electrodes. *ACS Nano* **2011**, *5*, 436–442.
47. Hu, L.; Choi, J. W.; Yang, Y.; Jeong, S.; La Mantia, F.; Cui, L.-F.; Cui, Y. Highly Conductive Paper for Energy-Storage Devices. *Proc. Natl. Acad. Sci. U. S. A.* **2009**, *106*, 21490–21494.
48. Kim, S.-K.; Choi, S.-W.; Jeon, W. S.; Park, J. O.; Ko, T.; Chang, H.; Lee, J.-C. Cross-Linked Benzoxazine-Benzimidazole Copolymer Electrolyte Membranes for Fuel Cells at Elevated Temperature. *Macromolecules* **2012**, *45*, 1438–1446.
49. Choi, B. G.; Hong, J.; Park, Y. C.; Jung, D. H.; Hong, W. H.; Hammond, P. T.; Park, H. S. Innovative Polymer Nanocomposite Electrolytes: Nanoscale Manipulation of Ion Channels by Functionalized Graphenes. *ACS Nano* **2011**, *5*, 5167–5174.